ELSEVIER

Theoretical and Applied Fracture Mechanics 29 (1998) 33–40

theoretical and applied fracture mechanics

Shear instability direction at a crack-tip in a thermoviscoplastic body

L. Chen, R.C. Batra *

Department of Engineering Science and Mechanics, Virginia Polytechnic Institute and State University, Blacksburg VA 24061-0219, USA

Abstract

Deformation fields near a crack tip are analyzed for a thermoviscoplastic body deformed either in an antiplane shear or in plane strain. The effects of inertia forces and heat conduction are considered, but those of material elasticity are neglected. By assuming that a shear band initiating from the crack-tip propagates in the direction of the maximum effective stress. It is found that a shear band propagates along the crack ligament in the body deformed in an antiplane shear. For a body undergoing plane strain deformations, the direction of the propagation of the shear band depends upon the mode-mixity parameter and agrees with that observed by Kalthoff.

Keywords: Antiplane shear; Plane strain deformation; Asymptotic fields; Mode-mixity parameter

1. Introduction

It was observed in [1,2] that shear bands form during the hot forging of a platinum bar. Research activity in the field increased since the observation [3] of a 20 μm wide shear bands during the punching of a hole in a low carbon steel plate. It was pointed out that the primary mode of deformation during the punching of a hole was simple shearing, and postulated that a material point became unstable when the hardening of the material due to strain and strain-rate effects equalled its softening due to the rise in its temperature (equivalently when the stress attained its maximum value). Since then this hypothesis has been adopted by several investigators [4–6]. Also, subsequent experimental, analytical and numerical work has shown that the strain at the instant of the initiation of the material instability depends upon the shape, size, and number of defects present in the body [7–10]. Defects considered include notches, thickness variation, weak elements, voids, rigid inclusions and second phase particles. Here we consider a very strong defect, namely a sharp crack and focus on ascertaining the direction along which a material instability initiating from the crack-tip will propagate. This work is motivated by the recent experimental work in [11,12] for a plate with two parallel cracks or notches and impacted by a cylindrical projectile of diameter equal to the spacing between the cracks. At high impact speeds, they observed that an adiabatic shear band propagates at approximately $-10°$ to the notch ligament. The study of adiabatic shear bands is important since they are usually followed by shear fractures.

An asymptotic analysis of the deformation fields near a crack-tip (e.g. see [13–15]) is performed in this work and angular distributions of stress-

* Corresponding author. Tel.: 540-231-6051; fax: 540-231-4574; e-mail: rbatra@vt.edu.

0167-8442/98/$19.00
PII: S0167-8442(98)00013-5

es and strain-rates in a thermoviscoplastic body deformed either in antiplane shear or in plane strain are obtained. Strain-rate hardening and thermal softening of the material are considered. Since we focus on analyzing deformation fields around the crack-tip, no initial-boundary value problem is analyzed. The direction of shear instability is assumed to coincide with that of the maximum effective stress, and for plane strain deformations is found to agree with the test values [11,12].

2. Formulation of the problem

Consider a cylindrical coordinate system (see Fig. 1) with origin at the crack-tip to study deformations of a thermoviscoplastic body subjected to either antiplane shear (i.e. mode III) or plane strain (mixed mode I and mode II) loading. Elastic deformations are neglected, and the material is assumed to be incompressible. This is reasonable since deformations near the crack-tip are expected to be large, and hence in the plastic range which generally are isochoric. The governing equations can be written as follows:

$$\rho\dot{\mathbf{v}} = \operatorname{div}\mathbf{S} - \nabla p, \tag{1}$$

$$\rho c\dot{T} = k\nabla^2 T + \operatorname{tr}(\mathbf{SD}), \tag{2}$$

$$\mathbf{S} = \kappa_0(1-\alpha T)(1+bI)^m\mathbf{D}\Big/\left(\frac{1}{2}I\right), \tag{3}$$

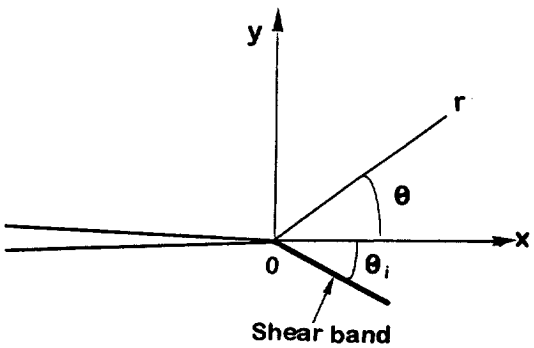

Fig. 1. A schematic sketch of the problem studied.

where ρ is the mass density, $\mathbf{v}$ the velocity, $\mathbf{S}$ the deviatoric Cauchy stress, p the hydrostatic pressure, c the specific heat, k the thermal conductivity, T the temperature rise, $\mathbf{D}$ the strain-rate tensor, κ_0 a strength parameter, α the thermal softening coefficient, b rate constant, m strain-rate sensitivity parameter, and $I \equiv (2\operatorname{tr}\mathbf{D}^2)^{1/2}$. All of the material parameters have positive values. Eqs. (1)–(3) are written in the spatial description, a superimposed dot indicates the material time derivative, ∇ is the gradient operator, ∇^2 the Laplacian, div the divergence and tr the trace. Eq. (1) expresses the balance of linear momentum and Eq. (2) the balance of internal energy. The balance of mass will be identically satisfied by the assumed velocity fields. Eq. (3), given in [16], generalizes Litonski's one-dimensional relation [17] to three-dimensional problems. It has been used [16] to study penetration problems; to analyze deformation fields around a shear band [18]; and to analyze the initiation and growth of shear bands [19]. Eq. (3) implies that $\left(\frac{3}{2}\operatorname{tr}\mathbf{SS}^{\mathrm{T}}\right)^{1/2} = \sqrt{3}\kappa_0(1-\alpha T)(1+bI)^m$ which is von-Mises yield criterion with the flow stress decreasing with a rise in the temperature but increasing with an increase in the strain-rate. Eq. (3) may be viewed as describing a non-Newtonian fluid with viscosity $(=\kappa_0(1-\alpha T)(1+bI)^m/I)$ a function of the strain-rate and temperature. However, for a fluid, the viscosity assumes a finite value at zero strain-rate but it is infinite for the material described by Eq. (3). Such constitutive relations have been used to model large deformations of metals e.g. see [20].

Assume that crack surfaces are traction free and are thermally insulated. Thus

$$\sigma_{\theta\theta}|_{\pm\pi} = \sigma_{\theta r}|_{\pm\pi} = \sigma_{\theta z}\Big|_{\pm\pi} = \frac{\partial T}{\partial\theta}\Big|_{\pm\pi} = 0, \tag{4}$$

where $\boldsymbol{\sigma} = -p\mathbf{1} + \mathbf{S}$ is the Cauchy stress tensor. Since the deformation fields around the crack-tip will be analyzed, therefore boundary conditions at surfaces far from the crack faces are not specified.

3. Shear instability in mode III deformations

In antiplane shear, only the out of plane component of velocity, $w(r,\theta,t)$, is non-zero. That is,

$$\mathbf{v} = (0, 0, w(r, \theta, t))$$

and the hydrostatic pressure, p, may be set equal to 0. In terms of w Eqs. (1)–(3) become:

$$\frac{\partial}{\partial r}\left(\frac{s}{I}\frac{\partial w}{\partial r}\right) + \frac{1}{r^2}\frac{\partial}{\partial \theta}\left(\frac{s}{I}\frac{\partial w}{\partial \theta}\right) + \frac{s}{rI}\frac{\partial w}{\partial r} = \rho\frac{\partial w}{\partial t}, \quad (5)$$

$$k\left[\frac{1}{r}\frac{\partial}{\partial r}\left(r\frac{\partial g}{\partial r}\right) + \frac{1}{r^2}\frac{\partial^2 g}{\partial \theta^2}\right] - \alpha s I = \rho c\frac{\partial g}{\partial t}, \quad (6)$$

$$I = \left[\left(\frac{\partial w}{\partial r}\right)^2 + \frac{1}{r^2}\left(\frac{\partial w}{\partial \theta}\right)^2\right]^{1/2}, \quad (7)$$

$$s = \kappa_0 g(1 + bI)^m, \quad (8)$$

$$g = 1 - \alpha T. \quad (9)$$

It is required that $0 \leqslant g \leqslant 1$.

A solution of Eqs. (5)–(9) in the immediate vicinity of the crack-tip just before the material there becomes unstable is sought. Assume that (e.g. see [21]):

$$w = f_1(t) r^a \tilde{w}(\theta), \quad (10)$$

$$s = f_2(t) r^b \tilde{s}(\theta), \quad (11)$$

$$g = g_0(t) + f_3(t) r^h \tilde{g}(\theta), \quad (12)$$

$$I = f_4(t) r^d \tilde{I}(\theta), \quad (13)$$

where $\tilde{w}$, $\tilde{s}$, $\tilde{g}$ and $\tilde{I}$ are non-dimensional functions of θ alone, a, b, h and d are constants, and f_1, f_2, f_3, f_4 and g_0 are dimensional functions of time t. $g_0(t)$ equals the value of the thermal softening function at the crack-tip, $0 < g_0(t) \leqslant 1$ prior to the initiation of the shear instability, and $h \geqslant 0$. Other forms of the thermal softening function do not yield a physically acceptable solution. Note that once a shear band has initiated, the solution near the crack-tip will generally be not of the type (10)–(13). Substitution from Eqs. (10)–(13) into Eqs. (5)–(9), assuming that $\dot{g}_0(t)$ and $\dot{f}_1(t)$ are bounded at the crack-tip, and requiring that the variable r drop out of each equation in the limit as $r \to 0$, yields coupled ordinary differential equations in θ for the angular functions in Eqs. (10)–(13). A consequence of the constitutive relation (8) and Eqs. (10)–(13) is that the near-tip fields are of HRR type [13,14,22]. That is

$$w = f(t) r^{\frac{m}{1+m}} \tilde{w}(\theta), \quad (14)$$

$$s = \kappa_0 b^m g_0(t) (f(t))^m r^{-\frac{m}{1+m}} \tilde{s}(\theta), \quad (15)$$

$$g = g_0(t)[1 + \alpha\kappa_0 b^m (f(t))^{m+1} r\tilde{g}(\theta)/k], \quad (16)$$

$$I = f(t) r^{-\frac{1}{m+1}} \tilde{I}(\theta), \quad (17)$$

and functions $\tilde{w}, \tilde{s}, \tilde{g}$ and $\tilde{I}$ satisfy

$$\tilde{w}'' + (m-1)\tilde{w}'\tilde{I}'/\tilde{I} + \frac{m}{(1+m)^2}\tilde{w} = 0, \quad (18)$$

$$\tilde{g}'' + \tilde{g} - \tilde{s}\tilde{I} = 0, \quad (19)$$

$$\tilde{s}^{1/m} = \tilde{I} = \left[\left(\frac{m}{1+m}\tilde{w}\right)^2 + (\tilde{w}')^2\right]^{1/2}, \quad (20)$$

where the amplitude factor $f(t)$ is assumed to be positive. A prime in Eqs. (18)–(20) indicates differentiation with respect to θ. In Eqs. (14)–(17), $f(t)$ has the dimensions (meter)$^{(1/1+m)}$/s. It can be verified that all equations are dimensionally correct. Note that all material parameters except the strain-rate sensitivity m drop out of Eqs. (18)–(20). Thus the asymptotic results at the crack-tip are valid for all rigid thermoviscoplastic materials obeying the flow rule (3). In the derivation of Eq. (19), $kf_3 = \alpha f_2 f_4$ is used. This implies that the amplitude of the strain-rate at the crack-tip is affected by thermal parameters k and α. However, thermal capacity and the mass density play negligible roles in the asymptotic solution. Since the motion is antiplane shear, therefore

$$\tilde{w}(0) = \tilde{g}'(0) = 0. \quad (21)$$

The boundary conditions (4) require that

$$\tilde{w}'(\pi) = \tilde{g}'(\pi) = 0. \quad (22)$$

The two second-order ordinary differential Eqs. (18) and (19) for $\tilde{w}(\theta)$ and $\tilde{g}(\theta)$ subject to boundary conditions (21) and (22) are solved over the interval $(0, \pi)$ by using the shooting method with a fourth-order Runge–Kutta integration scheme. The angular distributions of stresses, strain-rates and the thermal softening function around the crack-tip are depicted in Fig. 2(a)–(c)

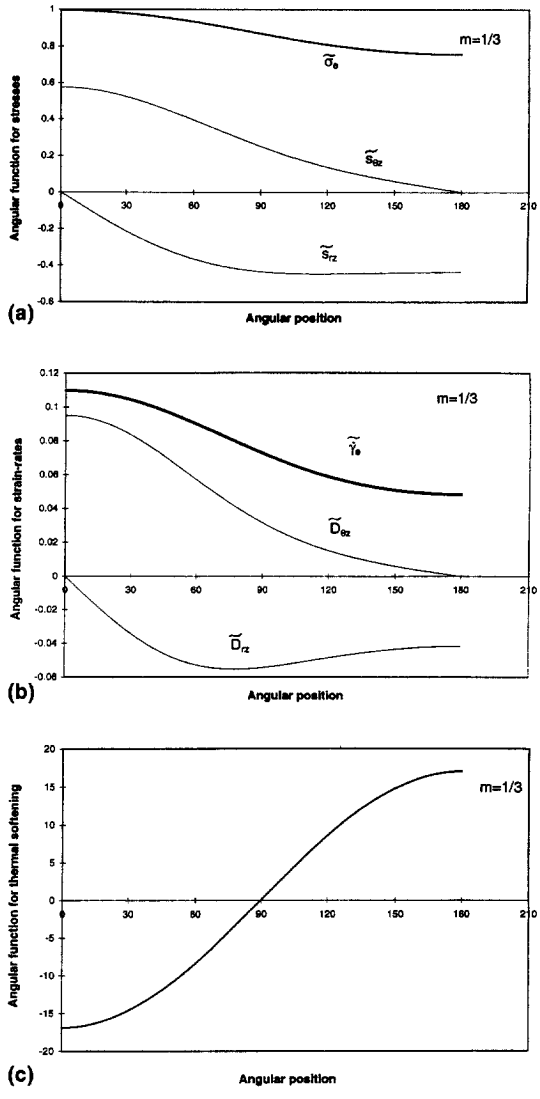

Fig. 2. Dependence upon the angular position in degrees of (a) stresses, (b) strain-rates and (c) the thermal softening function near the crack-tip for $m = 1/3$.

for $m = 1/3$; their amplitudes are determined by requiring that the maximum value of the effective stress, $\tilde{\sigma}_e = \left(\frac{3}{2}\,\mathrm{tr}(\tilde{\mathbf{S}}\tilde{\mathbf{S}}^{\mathrm{T}})\right)^{1/2}$, equals 1. It is evident that $\tilde{S}_{\theta z}$ and $\tilde{D}_{\theta z}$ are maximum at $\theta = 0$. Also the effective stress $\tilde{\sigma}_e$ and the effective plastic strain-rate $\dot{\gamma}_e \equiv \left(\frac{2}{3}\,\mathrm{tr}(\tilde{\mathbf{D}}\tilde{\mathbf{D}}^{\mathrm{T}})\right)^{1/2}$ are maximum at $\theta = 0$. Recall the work in [3] and assume that a material point becomes unstable when the effective stress there attains its maximum value. Thus, if we assume that a shear instability or a shear band propagates in the direction of the maximum effective stress then in a cracked thermoviscoplastic body deformed in antiplane shear, an adiabatic shear instability initiating at a crack tip will propagate along the crack ligament. This result is valid for all thermoviscoplastic materials that obey the flow rule (3). Because of the asymptotic analysis used, the result is valid in the immediate vicinity of the crack-tip and the direction of the shear band may change once it has propagated away from there. The variation of $\tilde{\sigma}_e$ vs. θ for $m = 1/13$ plotted in Fig. 3 suggests that the direction of propagation of the shear instability from the crack-tip is the same as that for $m = 1/3$, and probably is less sensitive to the value of m.

4. Shear instability in plane-strain deformations

Since the material studied herein is assumed to be incompressible, the continuity equation or the balance of mass,

$$\mathrm{tr}\,\mathbf{D} = 0, \tag{23}$$

is identically satisfied if the radial and tangential components u, v of the velocity $\mathbf{v}$ are defined as follows in terms of a stream function ϕ.

$$u = \frac{1}{r}\frac{\partial \phi}{\partial \theta} = \frac{1}{r}\phi_{,\theta}, \quad v = -\frac{\partial \phi}{\partial r} = -\phi_{,r}. \tag{24}$$

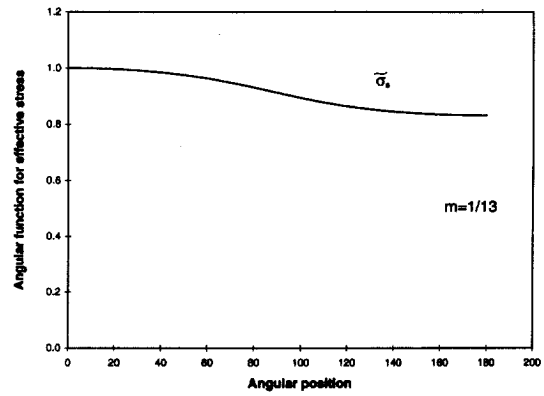

Fig. 3. Dependence upon the angular position in degrees of the effective stress near the crack-tip for $m = 1/13$.

Substitution from Eq. (24) into Eqs. (1)–(3) yields:

$$\frac{2}{r}\frac{\partial}{\partial r}\left(r\frac{s}{I}D_{11}\right)+\frac{2}{r}\frac{\partial}{\partial\theta}\left(\frac{s}{I}D_{12}\right)+\frac{2s}{rI}D_{11}-\frac{\partial p}{\partial r}=\rho\dot{u}, \tag{25}$$

$$\frac{2}{r}\frac{\partial}{\partial r}\left(r\frac{s}{I}D_{12}\right)-\frac{2}{r}\frac{\partial}{\partial\theta}\left(\frac{s}{I}D_{11}\right)+\frac{2s}{rI}D_{12}-\frac{1}{r}\frac{\partial p}{\partial\theta}=\rho\dot{v}, \tag{26}$$

$$k\left[\frac{1}{r}\frac{\partial}{\partial r}(rg_{,r})+\frac{1}{r^2}g_{,\theta\theta}\right]-\alpha sI=\rho c\dot{g}, \tag{27}$$

$$I=2(D_{11}^2+D_{12}^2)^{1/2}, \tag{28}$$

$$s=\kappa_0 g(1+bI)^m, \tag{29}$$

where

$$D_{11}=\frac{1}{r}\phi_{,r\theta}-\frac{1}{r^2}\phi_{,\theta}, \tag{30}$$

$$D_{12}=\frac{1}{2}\left(\frac{1}{r^2}\phi_{,\theta\theta}+\frac{1}{r}\phi_{,r}-\phi_{,rr}\right), \tag{31}$$

are deviatoric strain-rates. The non-zero components of the Cauchy stress tensor are given by

$$\sigma_{rr}=2\frac{s}{I}D_{11}-p, \tag{32}$$

$$\sigma_{\theta\theta}=-2\frac{s}{I}D_{11}-p, \tag{33}$$

$$\sigma_{r\theta}=2\frac{s}{I}D_{12}. \tag{34}$$

The elimination of pressure p from Eqs. (25) and (26) gives

$$\begin{aligned}&\frac{2}{r}\left(r\frac{s}{I}D_{11}\right)_{,r\theta}+2\left(\frac{s}{I}D_{11}\right)_{,r\theta}+\frac{2}{r}\left(\frac{s}{I}D_{12}\right)_{,\theta\theta}\\&\quad-2\left(r\frac{s}{I}D_{12}\right)_{,rr}+2\left(\frac{1}{r}\frac{s}{I}D_{11}\right)_{,\theta}-2\left(\frac{s}{I}D_{12}\right)_{,r}\\&\quad=(\rho\dot{u})_{,\theta}-(\rho r\dot{v})_{,r}.\end{aligned} \tag{35}$$

Assuming expressions (11), (12) and (13) for s, g and I, respectively, and

$$\phi=f_1(t)r^a\tilde{\phi}(\theta), \tag{36}$$

$$p=f_5(t)r^e\tilde{p}(\theta), \tag{37}$$

for ϕ and p, a reasoning similar to that used in the previous section gives expressions (15), (16) and (17) for s, g and I, respectively, and

$$\phi=f(t)r^{\frac{2m+1}{1+m}}\tilde{\phi}(\theta), \tag{38}$$

$$p=-\frac{1+m}{m}\kappa_0 b^m g_0(t)(f(t))^m r^{-\frac{m}{1+m}}\tilde{p}(\theta). \tag{39}$$

With Eqs. (15)–(17), (38) and (39), Eqs. (35), (27)–(29) and (25) can be written as follows:

$$\begin{aligned}&[1+(m-1)\tilde{I}^{-2}C^2]\tilde{\phi}''''+A(m-1)C/\tilde{I}\\&\quad+B+\frac{1+2m}{(1+m)^2}\tilde{\phi}''=0,\end{aligned} \tag{40}$$

$$\tilde{g}''+\tilde{g}-\tilde{s}\tilde{I}=0, \tag{41}$$

$$\tilde{s}^{1/m}=\tilde{I}=\left[4\left(\frac{m}{1+m}\right)^2(\tilde{\phi}')^2+C^2\right]^{1/2}, \tag{42}$$

$$\begin{aligned}\tilde{p}=&2\left(\frac{m(2+m)}{(1+m)^2}\right)\tilde{I}^{m-1}\tilde{\phi}'+(m-1)\tilde{I}^{m-2}\tilde{I}'C\\&+\tilde{I}^{m-1}C',\end{aligned} \tag{43}$$

where

$$C=\tilde{\phi}''+\left(\frac{1+2m}{(1+m)^2}\right)\tilde{\phi}, \tag{44}$$

$$\begin{aligned}A=&-\tilde{I}^{-3}\left[4\left(\frac{m}{1+m}\right)^2\tilde{\phi}'\tilde{\phi}''+CC'\right]^2\\&+\tilde{I}^{-1}\left[4\left(\frac{m}{1+m}\right)^2(\tilde{\phi}'')^2+4\left(\frac{m}{1+m}\right)^2\tilde{\phi}'\tilde{\phi}'''\right.\\&\left.+(C')^2+C\frac{1+2m}{(1+m)^2}\tilde{\phi}''\right],\end{aligned} \tag{45}$$

$$\begin{aligned}B=&4\left(\frac{m(m-1)}{(1+m)^2}\right)\tilde{I}^{-1}\tilde{I}'\tilde{\phi}'+4\frac{m}{(1+m)^2}\tilde{\phi}''\\&+\frac{m(2+m)}{(1+m)^2}C+(m-1)(m-2)\tilde{I}^{-2}(\tilde{I}')^2C\\&+2(m-1)\tilde{I}^{-1}\tilde{I}'C'.\end{aligned} \tag{46}$$

The boundary conditions (4) imply the following.

$$\tilde{\phi}''|_{\pm\pi} = -\frac{1+2m}{(1+m)^2}\tilde{\phi}|_{\pm\pi}, \tag{47}$$

$$\tilde{\phi}'''|_{\pm\pi} = -\frac{1+6m}{(1+m)^2}\tilde{\phi}'|_{\pm\pi}, \tag{48}$$

$$\tilde{g}'|_{\pm\pi} = 0. \tag{49}$$

Under mixed mode conditions, a near-field mixity parameter, M^p, defined as

$$M^p = \frac{2}{\pi}\tan^{-1}\left[\lim_{r\to 0}\frac{\sigma_{\theta\theta}(r,\theta=0)}{\sigma_{r\theta}(r,\theta=0)}\right] \tag{50}$$

has been introduced in [15]. It characterizes the relative contributions of modes I and II; $M^p = 0$ corresponds to pure mode II and $M^p = 1$ to pure mode I. The parameter M^p identifies all possible angular distributions of stresses, strain-rates and temperatures.

The fourth-order ordinary differential Eq. (40) for $\tilde{\phi}$ and the second-order ordinary differential Eq. (41) for $\tilde{g}$ under the boundary conditions (47)–(49) are solved by using the shooting method and the fourth-order Runge–Kutta integration scheme. Shih [15] pointed out that the shooting method and its variants are inadequate for the mixed mode analyses. It is found that for $\Delta\theta = 10^{-3}$ degree and $m = 1/13$, the shooting method performed well. The step size $\Delta\theta$ should be decreased for smaller values of m.

Figs. 4(a)–(c) depict the dependence upon θ of the angular functions for stresses, strain-rates and the thermal softening for $m = 1/3$ and $M^p = -0.22$; the amplitude has been determined by normalizing it so that the maximum value of $\tilde{\sigma}_e$ for $-\pi \leqslant \theta \leqslant \pi$ equals 1. It is clear that the effective stress and the effective plastic strain-rate are maximum at $\theta \simeq -5.8°$. Thus, according to the criterion stated in the previous section, a shear instability initiating from the crack-tip will propagate along $\theta = -5.8°$ for $m = 1/3$ and $M^p = -0.22$. The dependence of the angle θ_i along which a shear instability propagates upon the near-field mode-mixity parameter is exhibited in Fig. 5 for $m = 1/2, 1/3$ and $1/13$. These results evince that θ_i does not vary much with m, and

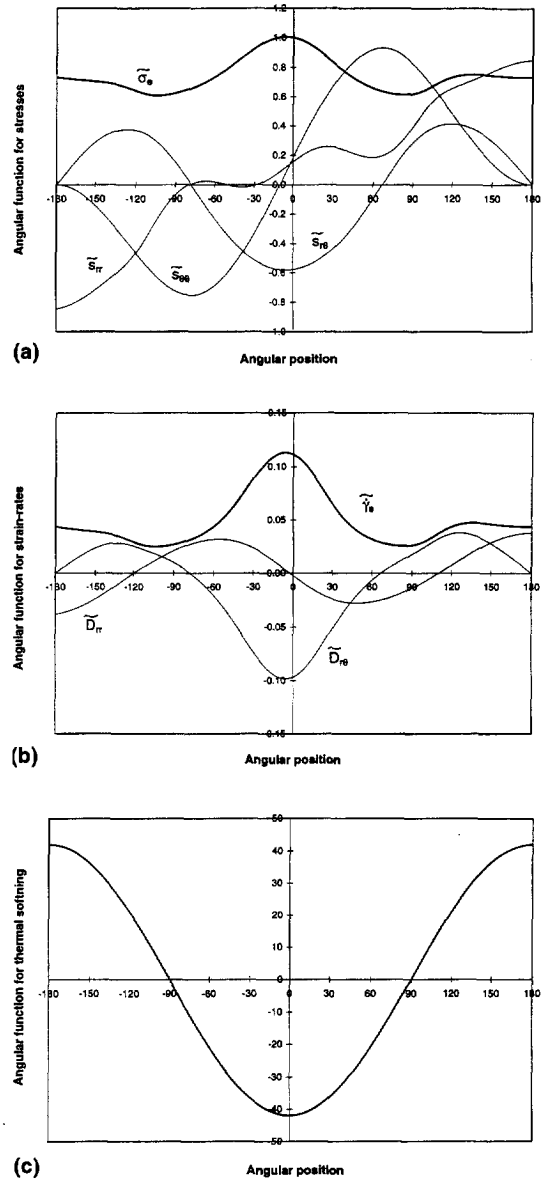

Fig. 4. Variation with the angular position in degrees of (a) stresses, (b) strain-rates and (c) the thermal softening function near the crack-tip for $m = 1/3$ and near-tip mode-mixity parameter $M^p = -0.22$.

$$\begin{aligned} \theta_i &= 0 \quad \text{for } M^p = 0, \\ \theta_i &= 95.6° \quad \text{for } M^p = 1. \end{aligned} \tag{51}$$

Thus, under pure mode II conditions near the crack-tip, a shear instability propagates along the

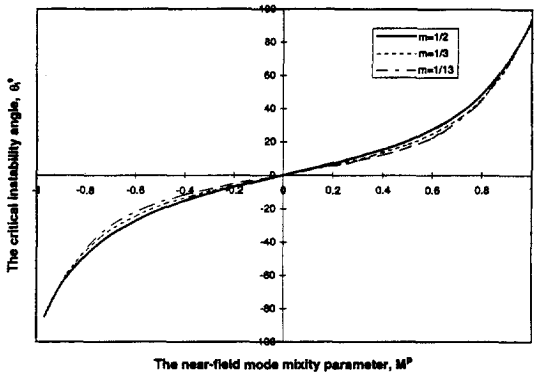

Fig. 5. Dependence of the direction of shear band upon the near-field mode-mixity parameter.

crack ligament, but under pure mode I conditions, it propagates along a direction that makes an angle of 95.6° to the crack ligament.

Another parameter, M^e [15] defined as

$$M^e = \frac{2}{\pi}\tan^{-1}\left[\lim_{r\to\infty}\frac{\sigma_{\theta\theta}(r,\theta=0)}{\sigma_{r\theta}(r,\theta=0)}\right] = \frac{2}{\pi}\tan^{-1}\left(\frac{K_I}{K_{II}}\right) \quad (52)$$

is introduced to characterize the relative strengths of K_I and K_{II} in the far-field under mixed-mode conditions. Here K_I and K_{II} are respectively the stress intensity factors under pure mode I and mode II loading. M^e equals 0 for pure mode II and $M^e = 1$ for pure mode I conditions in the far-field. The finite element method used in [15] to analyze the plane strain deformations of a power law hardening material; the computed relation between M^p and M^e is shown in Fig. 6. In this figure, only positive mixities are shown; the relationship between negative mixities can be extrapolated.

Time histories of stress intensity factors $K_I(t)$ and $K_{II}(t)$ for the experiments in [11, 12] are determined in [23], and imply that for the time interval of interest, the far-field mode-mixity parameter nearly equals -0.25 when Poisson's ratio for plate's material is 0.25. In Fig. 6, $M^e = -0.25$ corresponds to near-field mixities of about -0.43 to -0.30 for $1/13 \leqslant m \leqslant 1/2$. From Fig. 5, it can be concluded that for $1/13 \leqslant m \leqslant 1/2$, the direction of propagation of the shear instability will make an angle of approximately $-20°$ to $-10°$ with the crack ligament. This agrees reasonably well with Kalthoff's observation that a shear band propagates at $-15°$ to $-5°$ to the crack ligament.

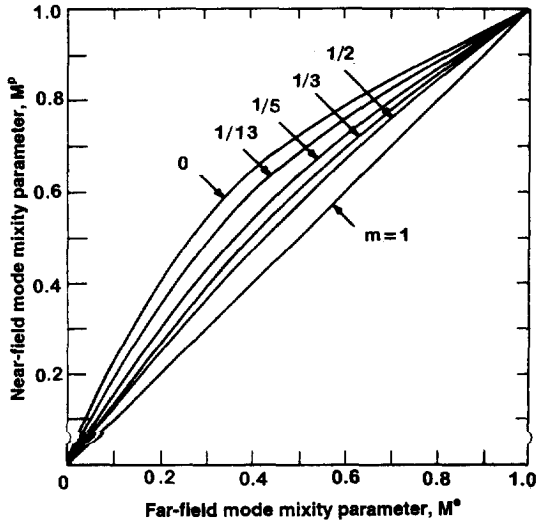

Fig. 6. Near-field mode-mixity parameter vs. far-field mode-mixity parameter for various values of m [15].

5. Conclusions

Asymptotic fields for the velocity, stress and thermal softening near a crack-tip are analyzed for a rigid thermoviscoplastic body deformed either in antiplane shear or in plane strain. Strain-rate hardening and thermal softening of the material are considered. Both for antiplane shear and plane strain deformations, the stresses and strain-rates are found to vary as $r^{-m/(1+m)}$ and $r^{-1/(1+m)}$ respectively where r is the distance from the crack-tip and m is the strain-rate hardening exponent. Stresses are also assumed to depend upon the temperature which takes on a maximum value at the crack-tip and decreases linearly with r. Assuming that a shear instability initiating at the crack-tip will propagate along the direction of the maximum effective stress, it is found that a shear instability will propagate along the crack ligament in a body deformed in antiplane shear. However, for a body undergoing plane strain deformations, the direction of propagation of the

shear instability depends upon the near-field mode-mixity parameter but not much on the strain-rate hardening exponent m. For loading conditions of Kalthoff's experiments and $1/13 \leqslant m \leqslant 1/2$, the angle between the direction of propagation of the shear instability and the crack ligament varies between $-20°$ and $-10°$ which is close to the observed values of $-15°$ to $-5°$.

Acknowledgements

This work was supported by the ONR grants N00014-94-1-1211 and N00014-98-1-0300 with Dr. Y.D.S. Rajapakse as the program manager.

References

[1] H. Tresca, On further application of flow of solids, Proc. Inst. Mech. Engr. 30 (1878) 301–345.
[2] H.F. Massey, The flow of metal during forging, in: Proc. Manchester Assoc. Engrs., 1921, pp. 21–26.
[3] C. Zener, J.H. Hollomon, Effect of strain rate on plastic flow of steel, J. Appl. Phys. 14 (1944) 22–32.
[4] R.F. Recht, Catastrophic thermoplastic shear, J. Appl. Mech. 31 (1964) 189–193.
[5] M.R. Staker, The relation between adiabatic shear instability strain and material properties, Acta Metall. 29 (1981) 683–689.
[6] R.J. Clifton, Adiabatic shear in material response to ultrahigh loading rates, in: W. Herrmann et al. (Eds.), NRC National Material Advisory Board (US) Report NMAB-356, Washington, DC, 1980.
[7] B. Deltort, Experimental and numerical aspects of adiabatic shear in a 4340 steel, J. Physique C8, 4 (1994) 447–452.
[8] A. Molinari, R.J. Clifton, Analytical characterization of shear localization in thermoviscoplastic materials, J. Appl. Mech. 5 (1987) 806–812.
[9] R.C. Batra, C.H. Kim, Analysis of shear bands in twelve materials, Int. J. Plasticity 8 (1992) 75–89.
[10] R.C. Batra, Z. Peng, Development of shear bands in dynamic plane strain compression of depleted uranium and tungsten targets, Int. J. Impact Eng. 16 (1995) 375–395.
[11] J.F. Kalthoff, Shadow optical methods of caustics, in: A.S. Kobayashi (Ed.), Handbook on Experimental Mechanics, Prentice-Hall, Englewood Cliffs, NJ, 1987, pp. 430–500.
[12] J.F. Kalthoff, S. Winkler, Failure mode transition at high strain rates of loading, in: C.Y. Chiem, H.D. Kunze, L.W. Meyer (Eds.), Proceedings of International Conference on Impact Loading and Dynamic Behavior of Materials, Deutsche Gewsellschaft für Metallkundcle, Bremen, 1988, pp. 185–196.
[13] J.R. Rice, G.F. Rosengren, Plane strain deformation near a crack tip in a power-law hardening material, J. Mech. Phys. Solids 16 (1968) 1–12.
[14] J.W. Hutchinson, Singular behavior at the end of a tensile crack in a hardening material, J. Mech. Phys. Solids 16 (1968) 13–31.
[15] C.F. Shih, Small-scale yielding analysis of mixed plane strain crack problems, Fracture Analysis, ASTM STP 560, 1974, pp. 187–210.
[16] R.C. Batra, Steady state penetration of thermoviscoplastic targets, Comp. Mech. 3 (1988) 1–12.
[17] J. Litonski, Plastic flow of a tube under adiabatic torsion, Bull. de l'Acad. Polonaise des Sciences 25 (1977) 7–17.
[18] T.W. Wright, J.W. Walter, The asymptotic structure of an adiabatic shear band in antiplane motion, J. Mech. Phys. Solids 44 (1996) 77–97.
[19] R.C. Batra, D.-S. Liu, Adiabatic shear banding in plane strain problems, J. Appl. Mech. 56 (1989) 527–534.
[20] O.C. Zienkiewicz, E. Onate, J.C. Heinrich, A general formulation for coupled thermal flow of metals using finite elements, Int. J. Numer. Methods Eng. 17 (1981) 1497–1514.
[21] L.B. Freund, Dynamic Fracture Mechanics, Cambridge Univ. Press, Cambridge, 1990.
[22] H. Riedel, Cracks loaded in anti-plane shear under creep conditions, Z. Metallkd 69 (1978) 755–760.
[23] Y.J. Lee, L.B. Freund, Fracture initiation due to asymmetric impact loading of an edge cracked plate, J. Appl. Mech. 57 (1990) 104–111.